Research Article Vol. 5, No. 4 / April 2018 / Optica 429

Transient nonlinear plasmonics in nanostructured graphene

Joel D. Cox[1,3] and F. Javier García de Abajo[1,2,4]

[1]ICFO—Institut de Ciencies Fotoniques, The Barcelona Institute of Science and Technology, 08860 Castelldefels (Barcelona), Spain
[2]ICREA—Institució Catalana de Recerca i Estudis Avançats, Passeig Lluís Companys 23, 08010 Barcelona, Spain
[3]e-mail: joel.cox@icfo.es
[4]e-mail: javier.garciadeabajo@nanophotonics.es

Received 5 December 2017; revised 5 March 2018; accepted 8 March 2018 (Doc. ID 315062); published 6 April 2018

Plasmons in highly doped graphene offer the means to dramatically enhance light absorption in the atomically thin material. Ultimately the absorbed light energy induces an increase in electron temperature, accompanied by large shifts in the chemical potential. This intrinsically incoherent effect leads to strong intensity-dependent modifications of the optical response, complementing the remarkable coherent nonlinearities arising in graphene due to interband transitions and anharmonic intraband electron motion. Through rigorous time-domain quantum-mechanical simulations of graphene nanoribbons, we show that the incoherent mechanism dominates over the coherent response for the high levels of intensity required to trigger nonperturbative optical phenomena such as saturable absorption. We anticipate that these findings will elucidate the role of coherent and incoherent nonlinearities for future studies and applications of plasmon-assisted nonlinear optics.

OCIS codes: (240.6680) Surface plasmons; (130.4310) Nonlinear; (190.7110) Ultrafast nonlinear optics.

https://doi.org/10.1364/OPTICA.5.000429

1. INTRODUCTION

Plasmon excitations in conducting nanostructures concentrate electromagnetic energy into spatial regions commensurate with the structure size, enabling control over light–matter interactions on the nanoscale for diverse applications including optical sensing [1,2], photovoltaics [3,4], and nonlinear optics [5,6]. In this context, highly doped graphene has emerged as an attractive plasmonic material capable of supporting long-lived and electrically tunable collective excitations that can boost light absorption well beyond the intrinsic broadband 2.3% level in pristine samples [7,8]. This material presents a $2E_F$ optical gap when doped to a Fermi energy E_F, and indeed, plasmons emerge within this gap, although, more realistically, they are severely damped by coupling to interband transitions unless the plasmon energy is $\lesssim E_F$. Under this condition, plasmons are well defined and supported by multiple coherently coupled virtual intraband transitions.

Currents associated with these intraband transitions undergo a strongly anharmonic motion that reflects the linear electronic dispersion in graphene and leads to a highly nonlinear response to external electromagnetic fields [9–17]. However, most experimental studies on graphene nonlinear optics have dealt with interband effects, including reports of large third-order susceptibilities linked to wave mixing [18], harmonic generation [19–23], and the Kerr effect [24–26]. Carbon monolayers are also an attractive platform for passive mode locking and other applications that rely on saturable absorption, which in undoped graphene emerges at remarkably low light intensities [27,28]. Although saturable absorption can be coherently induced, particularly in few-level molecular systems, the high optical intensities required to trigger this effect invariably lead to incoherent processes that substantially alter the response of a material such as graphene.

Similarly, incoherent processes can affect graphene plasmons: aside from the strong near-field enhancement, the optical energy absorbed upon resonant excitation of graphene plasmons and their eventual decay also elevates the temperature of its conduction electrons. The temperature increase can be dramatic because of the low heat capacity associated with massless Dirac fermions [29]. This phenomenon results in a delayed, *incoherent* nonlinear response, which can be exploited to optically modulate plasmon resonances. In particular, an intense ultrashort pump pulse can heat the 2D electron gas to an out-of-equilibrium state that reaches a local thermal equilibrium on a timescale of tens of femtoseconds, and subsequently cools by transferring energy to the graphene lattice at a much lower rate (~1 ps). Then, during the time when the electronic temperature has an elevated value, the response of graphene is characterized by transient plasmonic resonances that strongly affect optical absorption [29,30].

In this paper, we report on rigorous nonperturbative quantum-mechanical simulations to study the transient optical nonlinearity associated with plasmons in nanostructured graphene. We place the emphasis on the interplay between the coherent response of

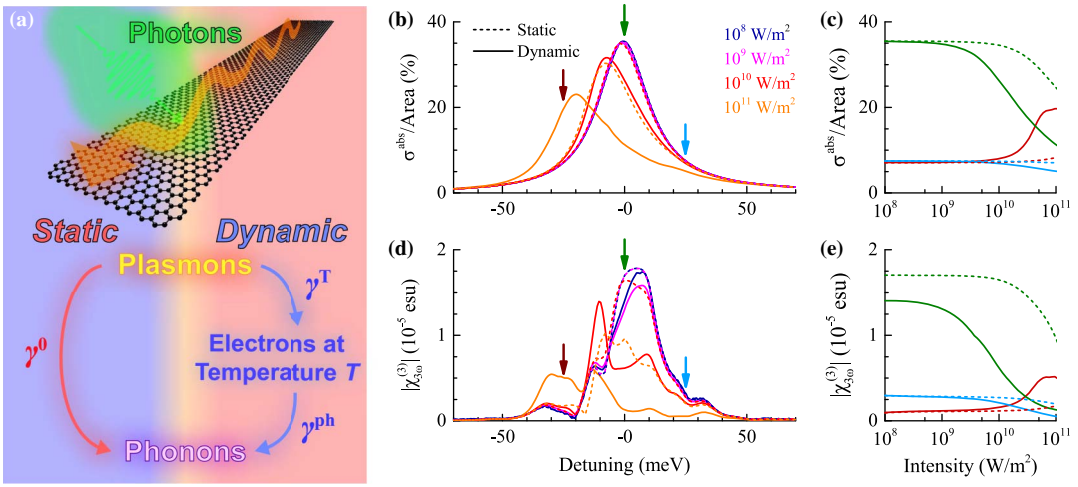

Fig. 1. Enhancement of saturable absorption and third-harmonic response by graphene plasmons under intense cw illumination. (a) Incident light excites plasmons in a graphene nanoribbon. Plasmon dissipation is usually described through direct inelastic decay to the initial electronic distribution at a rate γ^0 (static model, left). A more realistic description incorporates dynamic heating of the electrons at a rate γ^T before further relaxation to phonons at a rate γ^{ph} (dynamic model, right). (b) Normal-incidence absorption cross section of a highly doped (Fermi energy $E_F = 0.5$ eV) graphene nanoribbon (20 nm width) for different cw incident light intensities (upper-right legend), normalized to the graphene area. Light is polarized across the ribbon, which exhibits a transverse plasmon resonance of $\hbar\omega_p = 0.382$ eV energy (low intensity limit). The cross section is plotted as a function of detuning, defined as the photon energy relative to $\hbar\omega_p$. The results are obtained from self-consistent-field tight-binding simulations incorporating either the static ($\hbar\gamma^0 = 25$ meV, dashed curves) or dynamic ($\hbar\gamma^T = 20$ meV, $\hbar\gamma^{ph} = 5$ meV, solid curves) relaxation scheme. (c) Intensity dependence of the absorption cross section for three different photon energies, indicated by the color-coded arrows in (b). (d), (e) Third-harmonic susceptibility $\chi^{(3)}_{3\omega}$ in electrostatic units, assuming a 3.3×10^{-8} cm graphene thickness, under the same conditions as (b), (c).

the material and the incoherent effects produced when inelastic transitions transform part of the optically absorbed energy into electronic heat. Specifically, we consider graphene nanoribbons, which are common elements in both experimental studies and envisioned applications of graphene plasmonics [31–33]. We simulate the optical response of the ribbons using a tight-binding model for the electronic structure combined with self-consistent-field time-domain solutions of the one-particle density-matrix equation of motion [11,16]. Results are presented for continuous-wave (cw) illumination, individual ultrashort pulses, and degenerate pump–probe irradiation. With only a few reported measurements on the nonlinear plasmonic response of graphene [30,34], our work elucidates the role of electronic heating and out-of-equilibrium dynamics in optical absorption associated with graphene plasmons. In particular, we show that the incoherent response due to the out-of-equilibrium electronic distribution produces a remarkable reduction in the light intensity threshold for saturable absorption that persists over hundreds of femtoseconds, as revealed by pump–probe spectroscopy simulations.

2. THEORETICAL FORMALISM

Electron dynamics in graphene nanostructures is described by the single-electron density-matrix equation of motion [11,16]

$$\dot{\rho} = -\frac{\mathrm{i}}{\hbar}[H, \rho] - \Gamma(\rho),$$

where $H = H_{TB} - e\phi$ is the total Hamiltonian, consisting of the tight-binding term H_{TB} (with an assumed nearest-neighbor 2.8 eV hopping energy) and the interaction with the total electrostatic potential $\phi = \phi^{ext} + \phi^{ind}$, including contributions from the external driving electric field and the induced Coulomb interaction, respectively, and $\Gamma(\rho)$ describes incoherent electron scattering. The density matrix is constructed from single-electron states $|j\rangle$ with energies $\hbar\varepsilon_j$ according to $\rho = \sum_{jj'}\rho_{jj'}|j\rangle\langle j'|$, where $\rho_{jj'}$ are time-dependent complex-number coefficients. In practice, we express $\Gamma(\rho)$ by employing either of two levels of description [see Fig. 1(a)]: (i) a static relaxation scheme, consisting in directly relaxing the system at a phenomenological rate γ^0 to the equilibrium state corresponding to times before the external potential is introduced, so we take $\Gamma(\rho) = \gamma^0(\rho - \rho^0)$, where the matrix elements of ρ^0 are constructed as $\rho^0_{jj'} = \delta_{jj'}f_j$, with f_j denoting the occupations described by Fermi–Dirac statistics at ambient temperature (300 K in our simulations); and (ii) a dynamic relaxation scheme, in which the system relaxes at a fixed rate γ^T to a dynamically evolving equilibrium state that is determined by the instantaneous effective electronic temperature T and chemical potential μ, so we take $\Gamma(\rho) = \gamma^T(\rho - \rho^T) + \gamma^{ph}(\rho - \rho^0)$, where $\rho^T_{jj'} = \delta_{jj'}f_j(\mu, T)$ and the second term accounts for further relaxation to phonons at a rate γ^{ph}. In the dynamic relaxation scheme, T and μ are computed by imposing conservation of energy and electronic population, which lead to the equations

$$\sum_j \varepsilon_j[f_j(\mu, T) - f_j] = 0$$

and

$$2\sum_j f_j(\mu, T) = N_e,$$

respectively, with N_e denoting the number of electrons in the system. Comparison of the aforementioned treatments of electronic relaxation highlights the effect of out-of-equilibrium electron dynamics on the nonlinear plasmonic response of graphene.

3. RESULTS AND DISCUSSION

A. Continuous-Wave Illumination

Throughout this work, we consider a highly doped self-standing graphene nanoribbon ($W = 20$ nm width, zigzag edge

terminations, $E_F = 0.5$ eV Fermi energy) illuminated by light that is polarized across the ribbon width, focusing on the spectral range around the lowest-energy transverse dipole plasmon ($\hbar\omega_p = 0.382$ eV energy). In Fig. 1(b) we present absorption cross-section spectra corresponding to cw illumination with different light intensities. The cross section normalized to the graphene area A is obtained as $\sigma_\omega^{abs}/A = (4\pi\omega/cW)\mathrm{Im}\{p_\omega^{ind}/E^{ext}\}$ by first calculating the induced dipole p_ω^{ind} per unit of ribbon length for incident light of frequency ω and electric field amplitude E^{ext}. In the cw regime, the spectral weight of the impinging field is fully concentrated into each frequency considered, resulting in strong redshifting of the plasmon resonance when the out-of-equilibrium electron dynamics is taken into account. This phenomenon can be explained by the optically induced shift in the chemical potential attained in the steady-state, which modulates the effective plasmon resonance of the nanoribbon, while saturation of absorption dominates in the region near the original weak-field plasmon resonance. In Fig. 1(c), inspection of the absorption at the linear plasmon resonance frequency as a function of light intensity reveals a more rapid onset of saturable absorption in the dynamic relaxation scheme. We also show in Figs. 1(d) and 1(e) the effect of nonequilibrium dynamics on the nonlinear response associated with third-harmonic generation, which is found to be qualitatively similar to that on the absorption, but amplified through the higher-order dependence on the plasmonic near field.

B. Illumination by Intense Ultrashort Pulses

The electron temperature can rapidly increase in graphene under moderately intense resonant illumination because of the low heat capacity associated with Dirac fermions, a result originating in their conical dispersion, which also explains why only a small number of carriers is needed to sustain plasmons compared to materials with parabolic dispersion [29]. We investigate this phenomenon by studying the response to normally incident pulses of a fixed 1 J/m^2 fluence and varying full width at half-maximum (FWHM) duration Δ. The temporal evolution of different relevant quantities is presented in Figs. 2(a)–2(d) as obtained with the dynamic relaxation scheme. Specifically, we show the induced dipole moment [Fig. 2(a)], the total electronic energy [Fig. 2(b)], the chemical potential [Fig. 2(c)], and the electronic temperature [Fig. 2(d)] for pulses of duration $\Delta = 5$–160 fs (see labels). Although the pulse fluence is fixed, the energy delivered to the graphene nanoribbon increases with pulse duration [Fig. 2(b)] as a result of the involved Coulomb interactions among electrons, which persist in the absence of the driving incident field and produce an offset of the time at which a maximum is reached in the electronic energy. We note that remarkably large shifts in the chemical potential μ and electronic temperature T [Figs. 2(c) and 2(d)] are produced by using pulses of only 1 J/m^2 fluence, indicating a strong potential for efficient all-optical pulse modulation via pump–probe excitation of graphene plasmons.

Further insight into coherent and incoherent absorption is gained by analyzing the frequency-domain response associated with resonant pulse excitation. To this end, we plot in Figs. 2(e)–2(j) the spectral decomposition of the induced dipole moment for the pulses considered in Figs. 2(a)–2(d) (solid curves, dynamic relaxation scheme), along with that of the impinging pulses (dotted curves). The role of out-of-equilibrium dynamics is probed by superimposing data obtained from static relaxation simulations (dashed curves). For short pulses, different spectral components of the impinging pulse are absorbed in the dynamic and static relaxation schemes, although the total amount of absorbed energy is similar in both of them. In particular, the peak absorption frequency is blueshifted for pulses with a duration

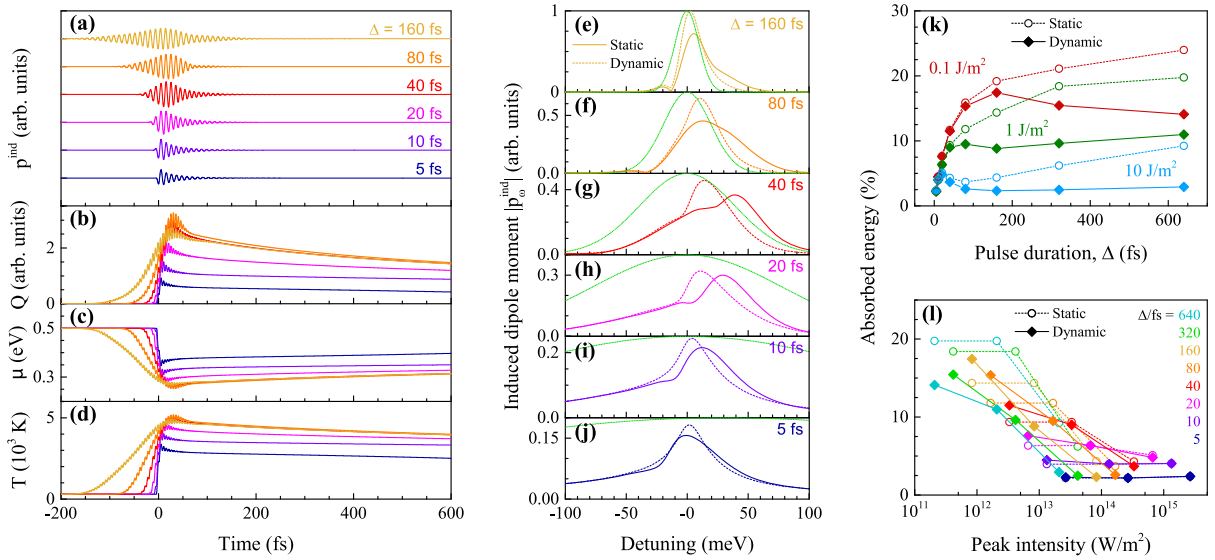

Fig. 2. Transient absorption of ultrashort light pulses tuned to a graphene plasmon. (a)–(d) Time-domain simulations showing the response of the nanoribbon considered in Fig. 1 to normally impinging Gaussian light pulses of varying FWHM duration Δ. The pulse central photon energy is tuned to the ribbon transverse plasmon ($\hbar\omega_p = 0.382$ eV), and the fluence is fixed to 1 J/m^2. We show (a) the induced dipole moment, (b) the electronic heat Q, (c) the chemical potential μ, and (d) the electronic temperature T. Results are obtained within the dynamic relaxation scheme [see Fig. 1(a)], assuming $\hbar\gamma^T = 20$ meV and $\hbar\gamma^{ph} = 5$ meV. (e)–(j) Spectral decomposition of the induced dipole moments under excitation by the pulses considered in (a)–(d), calculated in the dynamic (solid curves) and static ($\hbar\gamma^0 = 25$ meV, dashed curves) relaxation schemes and represented as a function of detuning (photon energy relative to $\hbar\omega_p$). The incident pulse spectra are shown for comparison (dotted curves). (k), (l) Fraction of energy absorbed from the directly impinging light (fluence times graphene area) as a function of either (k) pulse duration for the indicated pulse fluence or (l) peak intensity for different durations.

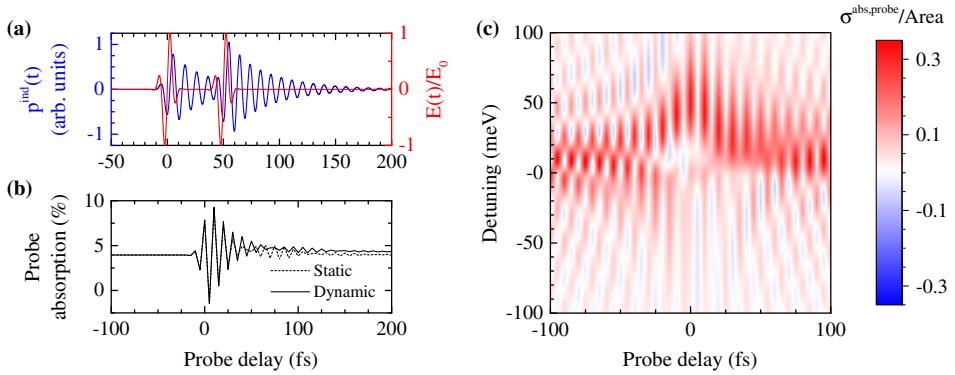

Fig. 3. All-optical modulation by transient graphene plasmons in a pump–probe configuration. (a) Induced dipole moment (left axis) upon pump–probe excitation (50 fs delay) of the ribbon in Fig. 1 using pulses tuned to the ribbon transverse plasmon, as calculated within the dynamic relaxation scheme. The incident light electric field is shown for comparison (right axis). (b) Fraction of energy absorbed from the directly impinging probe pulse calculated in the static (dashed curve) and dynamic (solid curve) relaxation schemes. (c) Spectral decomposition of the cross section for absorption of the probe pulse as a function of pulse delay and detuning. The pulse duration and fluence are 10 fs and 1 J/m^2 in all cases.

comparable to the relaxation time $1/\gamma^0$, such that most of the pulse overlaps temporally with the transient out-of-equilibrium electronic distribution, while the spectral response for longer pulses approaches the saturation and redshift observed under cw excitation [Fig. 1(b)]. Lower-fluence pulses, while still significantly decreasing the effective chemical potential, promote fewer electrons into excited out-of-equilibrium states, leading instead to a redshift of the effective nanoribbon plasmon frequency and increased absorption at lower frequencies (see Supplement 1 for more details).

The out-of-equilibrium electronic distribution clearly enhances the saturation of absorption, as illustrated in Figs. 2(k) and 2(l), in which we plot the normalized absorbed energy calculated from $(1/FA)\int \mathrm{d}t j^{\mathrm{ind}}(t)E(t)$, where $j^{\mathrm{ind}}(t)$ is the surface current induced by the impinging field $E(t)$, A is the graphene area, and F is the pulse fluence. The discrepancy between the predictions of the static and dynamic relaxation schemes increases with pulse duration and becomes dramatic for greater fluence. Likewise, greater fluence is required for saturation to occur as the pulse duration is decreased [Fig. 2(l)], so that it is hardly observable for the 5 fs pulses considered here, but reaches significant levels with pulses with a duration over a few tens of femtoseconds.

C. Pump–Probe Spectroscopy

The dramatic changes in the chemical potential and electronic temperature produced in the graphene nanoribbon by a resonant pump pulse can then be probed by a secondary pulse, as illustrated in Fig. 3. In particular, we simulate the modulation of a probe pulse by an identical pump pulse by varying the temporal separation between the two of them. For simplicity, we consider pulses of fixed duration ($\Delta = 10$ fs) and fluence ($F = 1$ J/m^2). In Fig. 3(a), we show the temporal evolution of the current $j^{\mathrm{ind}}(t)$ induced in the nanoribbon for a pump–probe delay of 50 fs, clearly revealing the overlap of the pump-induced current with the arrival of the probe. This results in a modulation of the energy absorbed from the probe as a function of delay, which is plotted in Fig. 3(b), as obtained from $(1/FA)\int \mathrm{d}t j^{\mathrm{ind}}(t)E^{\mathrm{probe}}(t)$, where $E^{\mathrm{probe}}(t)$ is the probe electric field amplitude. Pump modulation of the probe occurs for delays that are significantly longer than the duration of the induced current ($\sim 1/\gamma^T$, determined by inelastic relaxation of the plasmon field) as a result of changes due to the pump-induced out-of-equilibrium electronic distribution, extending up to delay times of $\sim 1/\gamma^{\mathrm{ph}} = 130$ fs for the assumed value of $\gamma^{\mathrm{ph}} = 5$ meV.

In practice, spectral information on the probe interaction can be gathered, for example, by sending pump and probe beams along slightly different directions near the graphene surface normal and spectrally decomposing the transmitted probe pulse. A simulation of this type of configuration is presented in Fig. 3(c) within the dynamic relaxation scheme, showing the cross section per unit of graphene area $\sigma_\omega^{\mathrm{abs,\,probe}}/A = (4\pi\omega/cW)\mathrm{Im}\{p_\omega^{\mathrm{ind}}/E_\omega^{\mathrm{probe}}\}$ in the frequency domain ω, where p_ω^{ind} is the spectral component of the total induced dipole moment per unit of ribbon length (i.e., produced by both pump and probe), while $E_\omega^{\mathrm{probe}}$ is the spectral component of the incident probe field [i.e., $\sigma_\omega^{\mathrm{abs,\,probe}}/A$ is defined in such a way that its frequency integral yields the profile shown in Fig. 3(b)]. The results reveal large variations in the probe absorption spectra, which remarkably include negative cross sections, representing stimulated photon emission (i.e., some of the probe components are amplified), as well as oscillations between emission and absorption with a detuning period $\omega - \omega_{\mathrm{p}} \sim 2\pi/\mathrm{delay}$. These variations become dramatic when illuminating with high-fluence pulses, with emission at certain spectral components appearing even at negative probe delay, that is, when the probe pulse arrives before the pump (see Supplement 1).

4. CONCLUSION

In summary, we have shown that the out-of-equilibrium electronic distribution induced by intense, resonant illumination of plasmons in nanostructured graphene results in a strong transient incoherent nonlinear optical response that can dominate over the sought-after coherent nonlinear response. Under such conditions, our results indicate that the combined changes in electronic temperature and chemical potential effectively detune the graphene plasmon resonances from their linear regime values, enabling all-optical modulation. Additionally, a significant saturation of absorption is predicted to occur due to such incoherent

processes, although in a more realistic scenario where the graphene nanostructure is supported by a substrate, screening by the dielectric environment should increase the required incident optical intensity. We attribute the reported high incoherent optical nonlinearity to the relatively low electronic heat of graphene and the comparatively small number of electrons involved in its plasmons, which limit the coherent nonlinear manipulation of optical pulses to very short durations (below 100 fs) but open new opportunities for transient plasmon-assisted light modulation, with potential uses in nonlinear nanophotonic devices such as optical switches and saturable absorbers.

Funding. Ministerio de Economía y Competitividad (MINECO) (MAT2017-88492-R, SEV2015-0522); European Commission (EC) (Graphene Flagship 696656); Catalan CERCA; Agència de Gestió d'Ajuts Universitaris i de Recerca (AGAUR) (SGR 2017-2019); Fundación Cellex.

See Supplement 1 for supporting content.

REFERENCES

1. K. Kneipp, Y. Wang, H. Kneipp, L. T. Perelman, I. Itzkan, R. R. Dasari, and M. S. Feld, "Single molecule detection using surface-enhanced Raman scattering (SERS)," Phys. Rev. Lett. **78**, 1667–1670 (1997).
2. J. N. Anker, W. P. Hall, O. Lyandres, N. C. Shah, J. Zhao, and R. P. Van Duyne, "Biosensing with plasmonic nanosensors," Nat. Mater. **7**, 442–453 (2008).
3. H. A. Atwater and A. Polman, "Plasmonics for improved photovoltaic devices," Nat. Mater. **9**, 205–213 (2010).
4. S. Linic, P. Christopher, and D. B. Ingram, "Plasmonic-metal nanostructures for efficient conversion of solar to chemical energy," Nat. Mater. **10**, 911–921 (2011).
5. M. Kauranen and A. V. Zayats, "Nonlinear plasmonics," Nat. Photonics **6**, 737–748 (2012).
6. J. Butet, P.-F. Brevet, and O. J. F. Martin, "Optical second harmonic generation in plasmonic nanostructures: from fundamental principles to advanced applications," ACS Nano **9**, 10545–10562 (2015).
7. R. R. Nair, P. Blake, A. N. Grigorenko, K. S. Novoselov, T. J. Booth, T. Stauber, N. M. R. Peres, and A. K. Geim, "Fine structure constant defines visual transparency of graphene," Science **320**, 1308 (2008).
8. K. F. Mak, M. Y. Sfeir, Y. Wu, C. H. Lui, J. A. Misewich, and T. F. Heinz, "Measurement of the optical conductivity of graphene," Phys. Rev. Lett. **101**, 196405 (2008).
9. S. A. Mikhailov, "Non-linear electromagnetic response of graphene," Europhys. Lett. **79**, 27002 (2007).
10. K. L. Ishikawa, "Nonlinear optical response of graphene in time domain," Phys. Rev. B **82**, 201402 (2010).
11. J. D. Cox and F. J. García de Abajo, "Electrically tunable nonlinear plasmonics in graphene nanoislands," Nat. Commun. **5**, 5725 (2014).
12. M. Jablan and D. E. Chang, "Multiplasmon absorption in graphene," Phys. Rev. Lett. **114**, 236801 (2015).
13. J. L. Cheng, N. Vermeulen, and J. E. Sipe, "Third-order nonlinearity of graphene: effects of phenomenological relaxation and finite temperature," Phys. Rev. B **91**, 235320 (2015).
14. T. Christensen, W. Yan, A.-P. Jauho, M. Wubs, and N. A. Mortensen, "Kerr nonlinearity and plasmonic bistability in graphene nanoribbons," Phys. Rev. B **92**, 121407 (2015).
15. S. A. Mikhailov, N. A. Savostianova, and A. S. Moskalenko, "Negative dynamic conductivity of a current-driven array of graphene nanoribbons," Phys. Rev. B **94**, 035439 (2016).
16. J. D. Cox, A. Marini, and F. J. García de Abajo, "Plasmon-assisted high-harmonic generation in graphene," Nat. Commun. **8**, 14380 (2017).
17. J. D. Cox, R. Yu, and F. J. García de Abajo, "Analytical description of the nonlinear plasmonic response in nanographene," Phys. Rev. B **96**, 045442 (2017).
18. E. Hendry, P. J. Hale, J. Moger, A. K. Savchenko, and S. A. Mikhailov, "Coherent nonlinear optical response of graphene," Phys. Rev. Lett. **105**, 097401 (2010).
19. N. Kumar, J. Kumar, C. Gerstenkorn, R. Wang, H.-Y. Chiu, A. L. Smirl, and H. Zhao, "Third harmonic generation in graphene and few-layer graphite films," Phys. Rev. B **87**, 121406 (2013).
20. S.-Y. Hong, J. I. Dadap, N. Petrone, P.-C. Yeh, J. Hone, and R. M. Osgood, Jr., "Optical third-harmonic generation in graphene," Phys. Rev. X **3**, 021014 (2013).
21. Y. Q. An, J. E. Rowe, D. B. Dougherty, J. U. Lee, and A. C. Diebold, "Optical second-harmonic generation induced by electric current in graphene on Si and SiC substrates," Phys. Rev. B **89**, 115310 (2014).
22. P. Bowlan, E. Martinez-Moreno, K. Reimann, T. Elsaesser, and M. Woerner, "Ultrafast terahertz response of multilayer graphene in the nonperturbative regime," Phys. Rev. B **89**, 041408 (2014).
23. A. Y. Bykov, T. V. Murzina, M. G. Rybin, and E. D. Obraztsova, "Second harmonic generation in multilayer graphene induced by direct electric current," Phys. Rev. B **85**, 121413 (2012).
24. R. Wu, Y. Zhang, S. Yan, F. Bian, W. Wang, X. Bai, X. Lu, J. Zhao, and E. Wang, "Purely coherent nonlinear optical response in solution dispersions of graphene sheets," Nano Lett. **11**, 5159–5164 (2011).
25. T. Gu, N. Petrone, J. F. McMillan, A. van der Zande, M. Yu, G. Q. Lo, D. L. Kwong, J. Hone, and C. W. Wong, "Regenerative oscillation and four-wave mixing in graphene optoelectronics," Nat. Photonics **6**, 554–559 (2012).
26. H. Zhang, S. Virally, Q. Bao, L. K. Ping, S. Massar, N. Godbout, and P. Kockaert, "Z-scan measurement of the nonlinear refractive index of graphene," Opt. Lett. **37**, 1856–1858 (2012).
27. Q. Bao and K. P. Loh, "Graphene photonics, plasmonics, and broadband optoelectronic devices," ACS Nano **6**, 3677–3694 (2012).
28. A. Marini, J. D. Cox, and F. J. García de Abajo, "Theory of graphene saturable absorption," Phys. Rev. B **95**, 125408 (2017).
29. F. J. García de Abajo, "Graphene plasmonics: challenges and opportunities," ACS Photon. **1**, 135–152 (2014).
30. M. M. Jadidi, J. C. König-Otto, S. Winnerl, A. B. Sushkov, H. D. Drew, T. E. Murphy, and M. Mittendorff, "Nonlinear terahertz absorption of graphene plasmons," Nano Lett. **16**, 2734–2738 (2016).
31. L. Ju, B. Geng, J. Horng, C. Girit, M. Martin, Z. Hao, H. A. Bechtel, X. Liang, A. Zettl, Y. R. Shen, and F. Wang, "Graphene plasmonics for tunable terahertz metamaterials," Nat. Nanotechnol. **6**, 630–634 (2011).
32. V. W. Brar, M. S. Jang, M. Sherrott, J. J. Lopez, and H. A. Atwater, "Highly confined tunable mid-infrared plasmonics in graphene nanoresonators," Nano Lett. **13**, 2541–2547 (2013).
33. M. S. Jang, V. W. Brar, M. C. Sherrott, J. J. Lopez, L. Kim, S. Kim, M. Choi, and H. A. Atwater, "Tunable large resonant absorption in a midinfrared graphene Salisbury screen," Phys. Rev. B **90**, 165409 (2014).
34. T. J. Constant, S. M. Hornett, D. E. Chang, and E. Hendry, "All-optical generation of surface plasmons in graphene," Nat. Phys. **12**, 124–127 (2016).